High-resolution ϕ-OFDR using phase unwrap and nonlinearity suppression

Zhen Guo, Jize Yan, Gaoce Han, Yifei Yu, David Greenwood and James Marco

***Abstract*—Phase-sensitive optical frequency domain reflectometer (ϕ-OFDR) is investigated to deliver an accurate distributed measurement with high spatial resolution. It is found that random phase noise and quadrant discrimination during phase calculation are the main reasons for the random hopping in ϕ-OFDR. By efficiently eliminating random hopping in the phase unwrap and suppressing the laser-induced nonlinear sweep for the theoretical spatial resolution, the proposed ϕ-OFDR is proved to be able to decouple the limitation between resolution and accuracy in coherent OFDR (C-OFDR). Distributed strain measurement with 20 mm spatial resolution in ϕ-OFDR is obtained and analysed. Measurement with little deviation and uniform sensitivity between applied strain and phase change both validate the efficient noise suppression for extreme resolution measurement. Then the influence of the initial sweep frequency between two times measurements is studied. With a further reduced 800 μm spatial resolution, the proposed ϕ-OFDR is able to retain accurate distributed measurement compared to conventional C-OFDR methods. Besides, the computation time of the ϕ-OFDR is only 3.2% of the C-OFDR.**

***Index Terms*—Distributed optical fibre sensor, phase-sensitive optical frequency domain reflectometer, resolution, accuracy**

I. Introduction

Resolution and accuracy are two essential sensing parameters in the distributed optical fibre sensor (DOFS) [1-3]. There is a trade-off among resolution, accuracy and time-frequency analysis in various DOFS [4,5]. In phase-sensitive optical time-domain reflectometers (ϕ-OTDR), excellent accuracy and sensitivity can be delivered by phase demodulation with a narrow linewidth laser. However, resolution in ϕ-OTDR is usually limited by the time-duration of the interrogated pulse and bandwidth of the digitizers [6-8]. As a comparison, millimetre/sub-millimetre sensing resolution can be realised in an optical frequency-domain reflectometer (OFDR) by sweeping the incident wavelength [9,10]. But the corresponding measurement accuracy is limited by the range of sweep wavelength, sample rate and laser nonlinear sweeping.

Compared to ϕ-OTDR, OFDR cannot directly detect phase variation using the wavelength sweeping method because both frequency and phase components are modulated in the interferometer of OFDR based on Rayleigh scattering, where the frequency corresponds to the position identification. Moreover, the cross-correlation in OFDR for calculating the frequency shift of the index variation induced by the environment variables (such as temperature/strain), also compromises the spatial resolution in high accuracy measurements [11,12]. In the coherent OFDR (C-OFDR), the theoretical relationship between the accuracy and spatial resolution is related to the incident wavelength and the fibre index [13]. Ref[14] proposed interpolation in the frequency domain to improve the distributed measurement accuracy. By effectively suppressing the nonlinear tuning and random wavelength sweep range, we previously delivered distributed strain measurement with ±0.51 με accuracy and 5 mm sensing resolution using C-OFDR [10].

Phase-sensitive OFDR (ϕ-OFDR) is an alternative OFDR technique, which measures phase spectrum variation. Unlike resolution comprised in the spatial filtering using cross-correlation, ϕ-OFDR has the potential to achieve the theoretical resolution by comparing the phase spectrum for the index variation tracking, which can be directly obtained by the fast Fourier transform [15]. Minimum measurable strain of 0.25 με was achieved using differential relative phases in ϕ-OFDR [16]. Multi-frequency detection was proposed to suppress the coherent fading to realize 0.55 με standard deviation and 5.6 cm spatial resolution [17]. For unwrap phase with low noise, a density distribution optimization is investigated to eliminate the phase hopping. Hundreds of με with the mm-level resolution were demonstrated for the distributed deformation measurement [18]. Inner-pulse frequency-division and rotated-vector-sum are proposed to suppress the weak fading point in the phase-detection distributed fibre optic vibration sensor with 35 km fibre length [19]. Besides, accurate measurement in C-OFDR usually leads to a long computation time due to the high calculation complexity of the cross-correlation in small spatial resolution.

ϕ-OFDR encountered severer phase noise compared to C-OFDR. Fine resolution measurement is more easily affected by many intrinsic noise, such as the laser phase noise, the nonlinear wavelength sweeping, the signal-to-noise ratio limitation and

Manuscript received XXXX, 2022; revised XXXX, 2022; accepted XXXX, 2022. Date of publication XXXX, 2022; date of current version XXXX, 2022.

This work was supported by the High Value Manufacturing Catapult and the Engineer and Physical Sciences Research Council - EPSRC EP/V000624/1. (Corresponding author: Zhen Guo)

Z. Guo, Y. Yu, D. Greenwood and J. Marco are with Warwick Manufacturing Group (WMG), University of Warwick, Coventry, CV4 7AL, United Kingdom; (e-mail: Zhen.Guo@warwick.ac.uk; Yifei.Yu.1@warwick.ac.uk; D.Greenwood@warwick.ac.uk; James.Marco@warwick.ac.uk).

J.Yan, G. Han are with Electronics and Computer Science (ECS), University of Southampton, Southampton, SO17 1BJ, United Kingdom; (e-mail: J.Yan@southampton.ac.uk; Gaoce.Han@southampton.ac.uk)

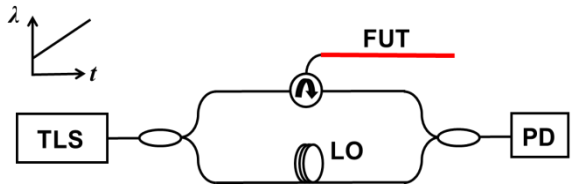

Fig.1 Schematic diagram of OFDR

the bandwidth of the digitizer. Moreover, unexpected random noise/hopping deteriorates measurement during the phase unwrapping. In this paper, we demonstrate that ϕ-OFDR could further expand the limitation between the resolution and accuracy in OFDR. The principle of ϕ-OFDR is first investigated in section II. The nonlinear laser sweep and random phase hopping are analysed and suppressed with proposed resample and filtering in section III. High accurate distributed sensing is demonstrated with the spatial resolution of 20 mm. In section IV, the influence of random initial sweep frequency and performance are compared to C-OFDR. 800 μm-level resolution is experimentally achieved.

II. Theory and Principle

The basic configuration of a coherent OFDR consists of a tuneable laser source (TLS) and an interferometer. By launching wavelength-sweep light into the fibre under test (FUT), a non-uniform distributed index along the fibre will induce Rayleigh back-scattering. Such scattering will interfere with the light from the local oscillator (LO) and can be digitized by a photo-detector (PD). Thus, with the wavelength-sweep speed of γ, the interference of position z along the fibre under test can be described as:

$$I(t) = E(z)^2 cos\left[2\pi\left(\upsilon_0\tau_z + \gamma\tau_z t - \frac{1}{2}\gamma\tau_z^2\right) + \varphi_n(t,\tau_z)\right] \quad (1)$$

where τ_z is the time delay between the position z in the fibre under test and the LO arm, υ_0 is the initial frequency, and ϕ_n is the phase noise. The position of z in the fibre under test would correspond to the beat frequency of $\gamma\tau_z$. With the finite wavelength sweep range, the theoretical spatial resolution of OFDR is $\Delta z = c/2n\upsilon_{sweep}$, where c is light speed, n is the index of fibre, and υ_{sweep} is the wavelength sweep range. In the strain measurement, the variation of the distributed permittivity in the fibre is introduced by filtering specific spatial relevant frequency components. This process is usually regarded as a sliding window in C-OFDR. Then, a cross-correlation of the filtered spectrum between the strained section and the same section without strain is conducted to compute the frequency shift for quantifying the applied strain. Thus, there is a resolution compromise during the sliding window and cross-correlation. The theoretical spatial resolution, initially determined by the wavelength sweep range, will be deteriorated hundreds/thousands of times to form sliding windows. A larger sliding window is usually preferred to guarantee measurement accuracy. Clearly, there is a trade-off between spatial resolution and strain measurement accuracy.

Applied strain will induce optical fibre length change, as shown in Fig. 2(a). The relationship between the length change and differential phase is [20]:

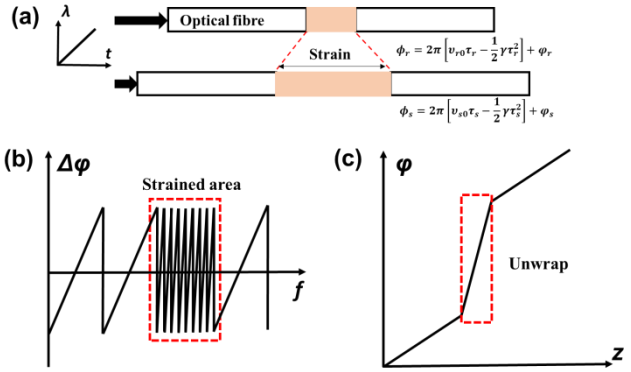

Fig.2 (a) Schematic diagram of phase sensitive OFDR (b) Phase spectrum difference with strained area (c) Unwrapping phase for distributed sensing.

$$\Delta\phi_z = \frac{4\pi}{\lambda_0}\left[(1 - P_e)n_{eff}\Delta L_z\right] \quad (2)$$

where P_e is the elasto-optic coefficient, λ_0 is the optical wavelength, n_{eff} is the effective refractive index, and ΔL_z is the corresponding length change. Thus, the differential phase $\Delta\phi_z$ is proportional to the length change caused by the applied strain. Phase demodulation enables OFDR with high accuracy. However, employed wavelength sweep in OFDR makes the received distributed back-scattering a sum of light with variations of frequency $\gamma\tau_z t$ and phase $\phi_n(t,\tau_z)$ (Eq.(1)). Therefore, classic phase demodulation, such as 3×3, PGC and heterodyne will not work. By Fourier transform of Eq. (1), the corresponding phase term can be expressed as:

$$\phi = 2\pi\left(\upsilon_0\tau_z - \frac{1}{2}\gamma\tau_z^2\right) + \phi_n(t,\tau_z) \quad (3)$$

which stands for the phase spectrum at corresponding position z. It needs two measurements step by step, one is noted to reference (r) and the other is sensing (s). Thus, as shown in Fig. 2 (a), the differential phase of $\Delta\phi = \phi_r - \phi_s$ is able to represent the length change induced by the applied strain. In the ideal assumption that the phase noise ϕ_n disturbance is omitted, the strain-free optical fibre only has a difference in the initial frequency of υ_{r0} and υ_{s0} ($\upsilon_0\tau_z \gg 1/2\gamma\tau z^2$). Thus, the differential phase $\Delta\phi$ is only proportional to the position z in the fibre under test, therefore, proportional to the corresponding frequency f (Fig. 2(b)). In the strained section, there will be an extra phase change caused by applied strain ΔL_z, as shown in Eq. (2). The differential phase can be unwrapped to quantitative represent the strain distribution along the optical fibre (Fig.2 (c)).

III. Experiment and Result

The experimental setup of ϕ-OFDR is shown in Fig.3. Santec-TSL-550 is a tuneable laser source with output power of 9.8 dBm. The wavelength sweep range is from 1555 nm to 1565 nm, therefore the theoretical spatial resolution is 82.19 μm. 99% light is split into the main interferometer, while the other 1% is into the auxiliary interferometer. Two 99:1 couplers are used to guarantee the sufficient light power into the fibre under test. A variable optical attenuator (VOA) is used to adjust the visibility

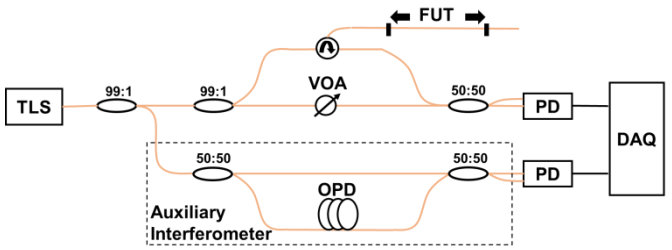

Fig. 3 ϕ-OFDR Experiment setup

of the interference. A 30-meters fibre Bragg grating (FBG) array is employed as fibre under test to enhance the Rayleigh back-scattering. A part of the FBG array is fixed on a strain applied stage for measurement and calibration. An additional temperature optical sensor is placed next to the fibre under test to compensate the temperature fluctuations.

An auxiliary interferometer is designed to compensate for the noise induced by the nonlinear laser sweep. The spatial resolution is a key figure of merit for OFDR, which is usually blurred by nonlinear laser sweep. Conventional zero crossing resampling by auxiliary interferometer is unable to achieve mm-level or μm-level resolution [21]. In our previous study, we proposed an equal frequency resample to suppress such noise for an ultimate theoretical spatial resolution of 12.1 μm [22]. In ϕ-OFDR based on differential phase spectrum, the realisation of such a theoretical resolution can be regarded as the baseline, as it makes sure the phase comparison happens at exact the same section during the two-step measurement.

With a 200 m long optical path delay (OPD) in the auxiliary interferometer and a proposed equal frequency resampling to eliminate the nonlinear tuning noise, the received time-domain signal is resampled and converted to the spatial domain by Fast Fourier transform. In Fig. 4(a), a 30-meters-long continuous reflection peak proves the enhanced Rayleigh back-scattering of the FBG array. Other peaks represent the positions of the connecters, circulators and splices in the optical circuit. Intensity drops to -110 dB noise ground at the end of 37 m fibre under test. The peak around 2.073 m in Fig.4 (b) is the connector of the single-mode fibre to the FBG array. The interface of two polished angle connectors can be regarded as an ideal index change with ultra-small resolution. The measured spatial resolution of this connector is 94.1 μm, following the theoretical prediction of a 10 nm wavelength sweep. It proves the effective suppression of the nonlinear laser sweep. By extracting the phase angle of both reference and sensing measurement, the corresponding phase spectrum is shown in Fig. 4(c). No useful information can be directly obtained from such a phase spectrum, because the summation of all reflected back-scattering has variations in both frequency and phase. Fig.4 (d) represents the differential phase between the reference and sensing measurement, which is better patterned than Fig.4 (c). The section from 4.01 m to 4.11 m is the fibre fixed on the strained stage. With an applied strain of 100 με, the differential phase behaves as a phase accumulation distribution compared to the strain-free section. The value of the differential phase is

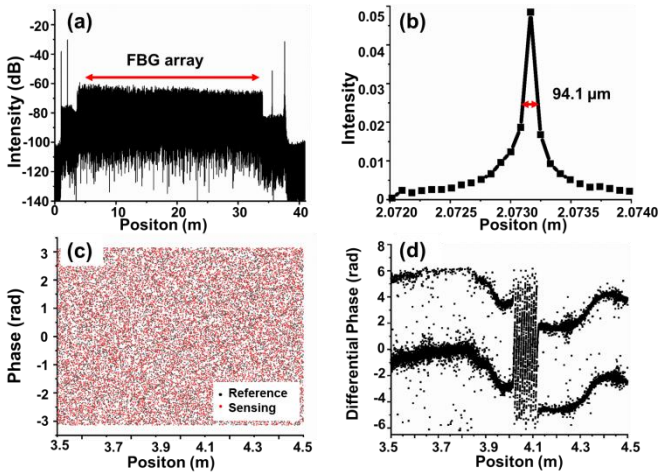

Fig.4 (a) Spatial domain distribution with 30 meters FBG array; (b) measured spatial resolution of 94.1μm under 10 nm wavelength sweep range; (c) phase spectrum of the reference and sensing measurement; (d) Differential phase distribution.

wrapped into the interval of [-2π, +2π). The mismatch of the initial phase between reference and sensing measurement will induce extra variation in the differential phase distribution. The zero-slope differential phase of the strain-free area in Fig. 4(d) has been optimized by post-processing calibration, which will be studied in the Discussion section. It is important to note every single point still stands for the theoretical spatial resolution. Therefore, it can be predicted that such ϕ-OFDR has the potential to realise μm-level resolution.

However, the differential phase spectrum is also inevitably affected by other factors, such as laser phase noise and digitiser noise. In the strain-free section, most of the wrap differential phases form two narrow bands with an interval of 2π. During the phase extraction from both measurements, the individual phase value is limited to [-π, π) due to the arctan calculation. Thus the differential phase would have a random 2π interval because of the quadrant discrimination. Such an interval does not affect the continuation of phase unwrapping. But the random phase lying in the medium area leads to undesired phase deterioration.

Phase unwrapping is implemented to represent better the phase variation induced by the externally applied strain. In Fig. 5(a), discriminated interval of 2π is efficiently removed during unwrapping. There is an apparent phase accumulation within the strained section from 4.01 m to 4.11 m. The accumulated unwrap value is around 65 rad. But unexpected random phase hopping exists all along the fibre, which will distort the distributed measurement. Take random hopping around 3.943m, for example. The zoom-in of the differential phase distribution is shown in Fig. 5(b). To the phase hopping at 3.9428 m, the corresponding differential phase is 0.899. In the process of phase unwrapping, the calculated phase difference to the previous point is 3.3269, which is less than 2π. Thus, an algorithm of unwrapping wrongly represents a phase accumulation of 3.3269 at this position. But there is no actual strain applied to that specific point. Therefore, random phase noise and quadrant discrimination during unwrapping could be the main reasons for the unexpected unwrap hopping.

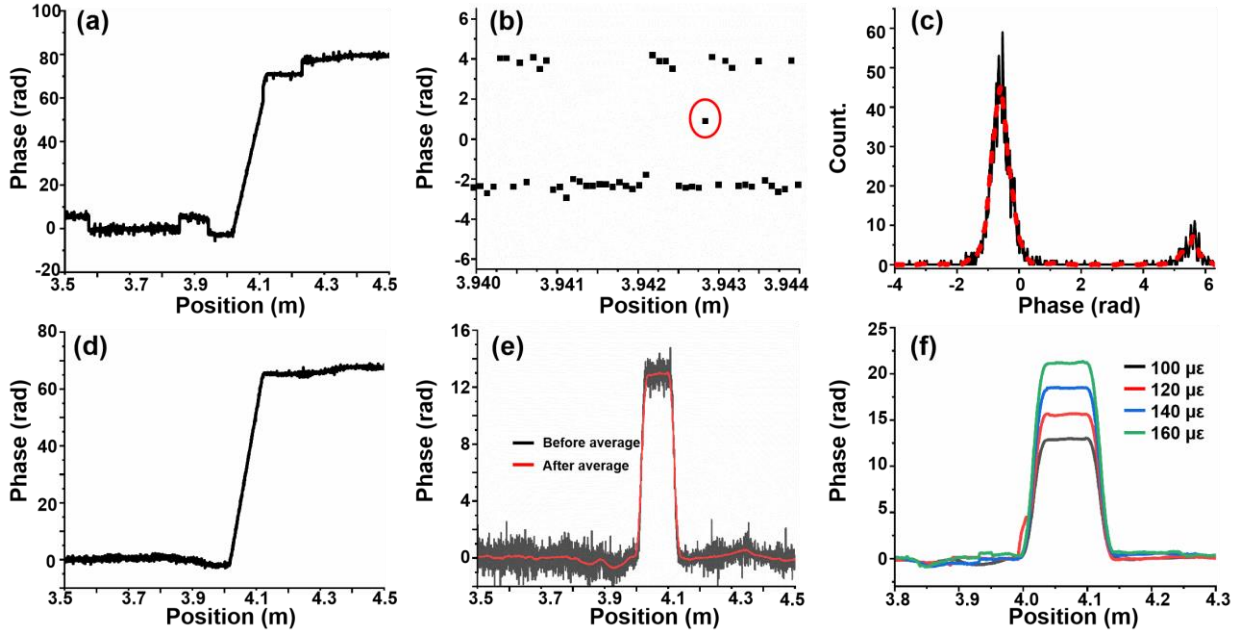

Fig.5 (a) Unwrap of differential phase; (b) Zoom of differential phase around the hopping of 3.943 metre; (c) Statistic distribution of differential phase from 3.5m to 3.6 m; (d) corrected unwrap of differential phase; (e) Distributed stain measurement comparison with 20 mm resolution average; (f) Distributed measurements with various applied strain.

The strain measurement range is determined by the phase unwrapping value of π. If applied strain induced phase shift to the fibre segment exceeds π, the ϕ-OFDR will not be able to distinguish the actual applied-strain. The average phase difference has a linear relationship with the fibre segment under 100 με applied strain, as shown in Fig. 4(d). The slope is about 0.000508196 rad/με under a spatial resolution of 82.19 μm. Thus the unwrapping threshold of π determines the ± 6,178 με measurement range. This value also agrees to the C-OFDR prediction with 10 nm sweep range and usual 100 MHz/με sensitivity.

In our setup, phase noise mainly comes from laser linewidth, digitizer noise and nonlinear sweep noise. Nonlinear sweep noise has been discussed above and compensated to achieve the theoretical spatial resolution. The Fourier transform of the OFDR measurement is [13]:

$$\check{I} = \frac{1}{N}\sum_{j=0}^{N-1} I\ exp\left(-imj\frac{2\pi}{N}\right)\ \ at\ \Delta z = \frac{c}{2\pi v} \qquad (4)$$

However, with the increasing length of the fibre under test, there will be inevitable accumulation phase error to blur the phase spectrum, such as random wavelength sweep range υ [10] and jitter in the digitizer. Therefore, instead of subtraction of entire spectrum for phase difference, the spectrum can be divided into small sections in advance. It will help to calibrate the frequency distribution and eliminate noise accumulation. The method is better than the spatial filtering of the sliding window in C-OFDR and does not compromise the resolution and not induce extra calculation complexity. The length of each divided section is 0.1m, which means there are about 1220 theoretical-resolution points in each section.

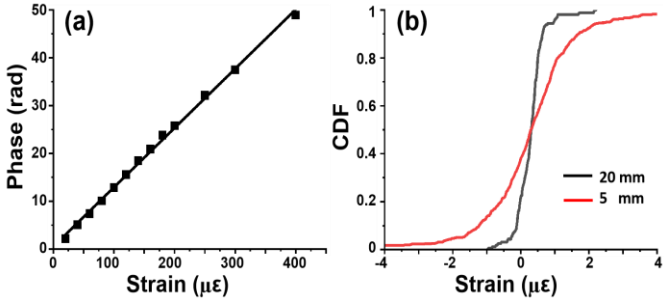

Fig.6 (a) Sensitivity between applied strain and phase with a 20 mm spatial resolution (b) Cumulative distribution function (CDF) with the resolution of 20mm and 5mm.

Unwrap hopping happens due to the phase discrimination of specific points, which randomly lie between the 2π-interval narrowband (Fig. 5(b)). Thus, such hopping can be eliminated by post-filtering. At first, the phase distribution along the fibre under test is statistically analysed and forms two main bands, covering most of the regular points. Such two bands ought to have an average difference of 2π. Then, the distance of each point to the corresponding central bands is calculated and evaluated. The set of distances should behave like a Gaussian distribution. Finally, points beyond a certain distance to the band centre will be eliminated because such points are more likely to induce unwrap hopping. Fig.5 (c) shows the statistic distribution of the differential phase value of one section from 3.5 m to 3.6 m. Most of the differential phase lies around the peak of -0.61 and 5.53. Based on the proposed filtering, values ranked outsides the 3σ width to the centre will be eliminated. Fig.5 (d) represents the optimized phase unwrap by the proposed method. There is no more phase hopping along the fibre under test compared to Fig. 5(a). Besides, the strained area from 4.05m to 4.15m is barely affected with additional optimization, and whose accumulated phase is still around 65.56 rad.

Even though the unwrap phase hopping can be efficiently suppressed in Fig. 5(d), the residual phase noise is still too high to distinguish the strain distribution at the theoretical resolution which is 82.19 μm. Therefore, a further data-smooth filter is

utilized. It is noted such a filter would lead to resolution deterioration. The black curve in Fig. 5(e) shows the distributed strain measurement after the data-smooth filter. The length of one filter is 243, indicating the actual measurement resolution is 20 mm. The further average is introduced and shown as the red curve in Fig. 5(e). Applied strain of 100 με causes 12.93 rad phase change along the stretch fibre segment. The distributed measurement with various applied strain is also shown in Fig. 5(f). With the applied strain of 120 με, 140 με, and 160 με, the measurement phase change is 15.62, 18.54 and 20.98, respectively. The sensitivity coefficient between the applied strain and measured differential phase is studied in Fig. 6(a). The resolution is 20 mm, and the wavelength sweep range is 10 nm. The slope of the curve represents the sensitivity coefficient, which is 0.124 rad/με. The R-square, coefficient of determination, is introduced to represent the linearity of the sensitivity coefficient. The value of R-square is 0.9982, proving the high fidelity and linearity between the applied strain and measured phase shift.

In order to further quantify the measurement accuracy, the cumulative distribution function (CDF) is employed to represent the measurement accuracy. Mounts of phase shifts of the strained and un-strained area are measured multiple times for the random deviation investigation. The phase shift of the strained area needs to subtract the mean value caused by the applied strain. The measurement accuracy is defined as the 2σ standard deviation of the random phase shift. This accuracy represents the closeness of measurements to a specific value of applied strain. Therefore, in Fig. 6(b), the measurement accuracy is about 1.76 με with a 20 mm resolution and 6.71 με with a 5 mm resolution.

Uniform measurement with small deviation and linear sensitivity coefficient between applied strain and measured phase validate efficient suppression of phase noise, proving ϕ-OFDR a potential way to further extend the boundary of both resolution and accuracy.

IV. Discussion

ϕ-OFDR has the potential to realise the theoretical spatial resolution by differential phase spectrum. But such phase-sensitive demodulation not only encounters phase noise, but is also affected by the employed wavelength sweeping. As show in Eq. (3), there is a constant $\upsilon_0\tau_z$ related to the initial sweep frequency. Such initial frequency variation between two step measurements $\Delta\phi=(\upsilon_{r0}-\upsilon_{s0})\tau_z$ determines the slope of the wrap differential phase. Fig.7 (a) shows one of the multiple tests under the same parameters and setup above. Compared to Fig. 4(d), the slope of the wrapped phase in Fig.7 (a) increases with the mismatch of the initial frequency. This is mainly caused by the finite synchronization of the tuneable laser source and sampling of the DAQ. Such initial frequency mismatch at each laser sweep is random and inevitable. A steep slope could produce more discrimination points together with phase noise. This will lead extra burden for the proposed filtering. Fig. 7(b) shows the corresponding distributed strain measurement after an average of 20mm sensing resolution. There are two phases hopping around 3.6m and 3.8m and one hopping in the strained area. Thus, extra synchronization between two step (reference and sensing) measurements should be taken into consideration to make sure the identical sweeping frequency. Such initial frequency inconsistency can be monitored by wavelength calibration like a gas absorption cell [17] or a post-data calibration.

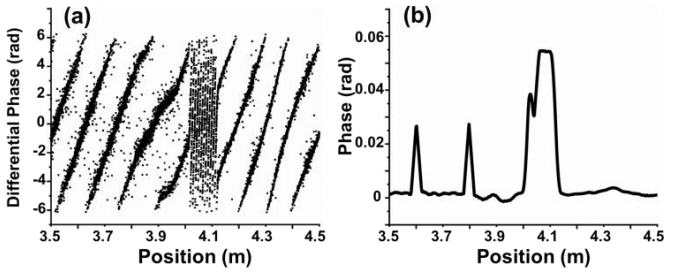

Fig.7 (a) Differential phase distribution with random initial frequency of $\Delta\upsilon_0=\upsilon_{r0}-\upsilon_{s0}$; (b) Deteriorate strain measurement without initial frequency calibration.

Fig. 8 represents the comparison between C-OFDR and ϕ-OFDR in terms of spatial resolution. The experimental relationship between measurement accuracy and resolution by

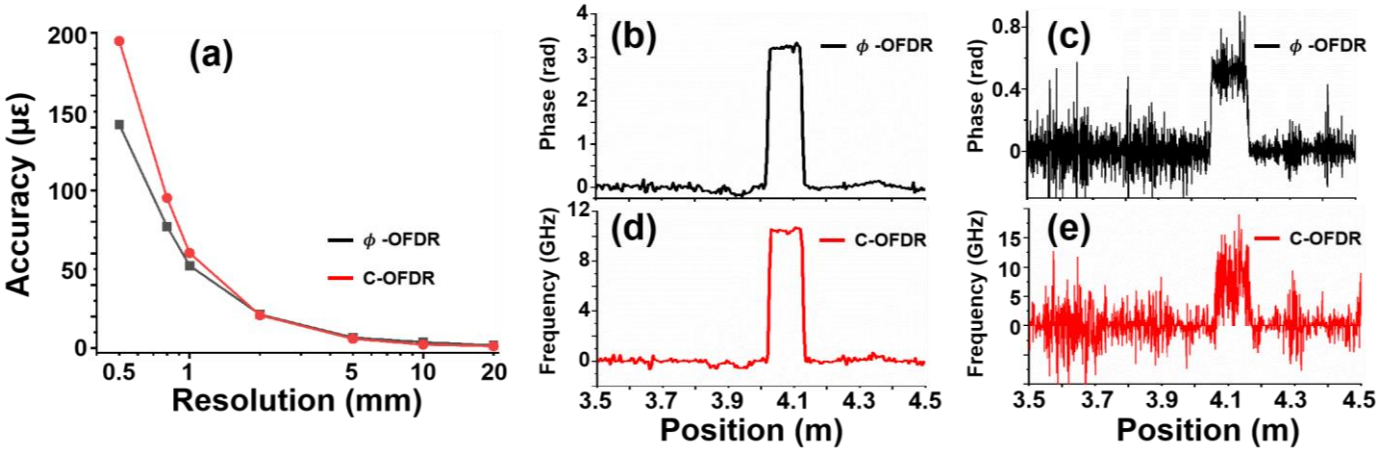

Fig.8 (a) Relationship between the measured strain accuracy and spatial resolution in C-OFDR and ϕ-OFDR. Under a 100με applied strain (b) ϕ-OFDR with 5 mm sensing resolution; (c) ϕ-OFDR measurement with 800 μm sensing resolution; (d) C-OFDR measurement with 5 mm sensing resolution; (e) C-OFDR measurement with 800 μm sensing resolution.

proposed method has been shown in Fig. 8(a). The wavelength sweep range is 10nm at 100nm/s speed. The measurement accuracy is 1.76 με with a 20 mm resolution in ϕ-OFDR, while the C-OFDR accuracy is 1.26 με. Both measurement accuracy deteriorates exponentially with the decreasing sensing resolution, which agrees with the prediction of the C-OFDR [13]. With the ultimate resolution of less than 1 mm, the proposed ϕ-OFDR can deliver a more accurate measurement to conquer the limitation in C-OFDR. When the spatial resolution is 0.5 mm, the measurement accuracy in ϕ-OFDR is 141.27 με, while the accuracy is only 194.66 με with C-OFDR. The sensing resolution is 5 mm in Fig. 8(b) and (d). In ϕ-OFDR, a 5 mm sensing resolution determines the length of the data-smooth filter is 61. In C-OFDR, the theoretical frequency resolution is 20.56 GHz. Therefore, in each 5 mm-resolution calculation, multiple times of zero are needed to be padded at the end of the sliding window for any 1με strain resolution (about 100 MHz/με). Both ϕ-OFDR and C-OFDR can deliver an accurate distributed strain measurement. But the sensing resolution of ϕ-OFDR is further reduced to 800 μm (Fig. 8(c)). There are random phase hopping in ϕ-OFDR, indicating the necessity of further optimization of the phase hopping filter. However, the area and the value of applied strain on the fibre segment can be distinguished. Apart from the phase hopping, the deviation of distributed measurement in ϕ-OFDR is much smaller than C-OFDR in Fig. 8(e). The deteriorated measurement with severe random deviation shown in Fig. 8 (e) demonstrates the limitation in C-OFDR, proving that ϕ-OFDR is able to deliver better sets of resolution and accuracy.

The other advantage of ϕ-OFDR is the elimination of cross-correlation in each sliding window. For a better spatial resolution, the calculation of the amounts of cross-correlation consumes the computation time significantly in C-OFDR. Instead, just one fast Fourier transform and phase subtraction is sufficient for ϕ-OFDR, making the distributed dynamic measurement with better resolution and accuracy possible in ϕ-OFDR. In the experimental setup of the Intel Core i7-6700 CPU, 16 GB RAM and the spatial resolution is 20mm, the computation time of C-OFDR demodulation is 14.04 seconds, while the computation time of ϕ-OFDR demodulation is only 0.45 seconds, about 3.2% time consuming compared to C-OFDR. Such improvement can also be theoretically explained by the Generalized Stokes Theorem over one dimension manifold (Fundamental theorem of calculus):

$$\int_M d\omega = \int_{\partial M} \omega \tag{5}$$

where the complicated frequency integral over a certain position/frequency and a certain time (i.e. sliding window and cross-correlation) is efficiently replaced by a direct calculation of phase difference induced by the applied strain.

Intrinsic phase noise will become more dominant with the further reduced resolution and/or long-distant fibre under test. Thus, for the stable measurement with μm-level resolution in ϕ-OFDR, the tuneable laser source with narrower linewidth and efficient phase noise suppression is more desirable.

V. CONCLUSION

μm-level spatial resolution is a crucial feature of OFDR in various practical applications, such as optical coherent tomography, three-dimensional coordinate measurement, and battery monitoring. However, such resolution can only be achieved with compromised measurement accuracy in C-OFDR, due to the sliding window for calculating the frequency shift and limited relationship between silicon-based fibre sensitivity (i.e. 100 MHz/με) and sweep wavelength range. By efficiently suppress the nonlinear sweep noise and random unwrap phase hopping using equal frequency resample and optimized filtering, proposed ϕ-OFDR has been proved to retain improved sets of spatial resolution and measurement accuracy. Besides, a more concise and straightforward demodulation in ϕ-OFDR reduces the computation time significantly compared to C-OFDR.

REFERENCES

[1]. N. David, P. Wild, J. Hu and N. Djilali, "In-fibre Bragg grating sensors for distributed temperature measurement in a polymer electrolyte membrane fuel cell, " *Journal of Power Sources*, vol. 192, no. 2, pp. 376-380, 2009.

[2]. Y. Koyamada, M. Imahama, K. Kubota and K. Hogari, "Fiber-Optic Distributed Strain and Temperature Sensing With Very High Measurand Resolution Over Long Range Using Coherent OTDR," *J. Lightwave Technol*, vol. 27, no. 9, pp. 1142-1146, 2009.

[3]. T. Horiguchi, K. Shimizu, T. Kurashima, M. Tateda, and Y. Koyamada, "Development of a distributed sensing technique using Brillouin scattering," *J. Lightwave Technol*. vol. 13, no. 7, pp. 1296–1302, 1995.

[4]. P. Lu, N. Lalam, M. Badar, B. Liu, B. T. Chorpening, M. P. Buric, and P. R. Ohodnicki, "Distributed optical fiber sensing: Review and perspective," *Applied Physics Reviews*, vol. 6, no. 4, 041302, 2019.

[5]. Y. Yu, L. Luo, B. Li, K. Soga and J. Yan, "Frequency Resolution Quantification of Brillouin-Distributed Optical Fiber Sensors," *Photonics Technology Letters*, vol. 28, no. 21, pp. 2367-2370, 2016.

[6]. F. Peng, H. Wu, X.Jia, Y.Rao, Z. Wang, and Z. Peng, "Ultra-long high-sensitivity Φ-OTDR for high spatial resolution intrusion detection of pipelines," *Opt. Express*, vol. 22, no. 11, pp. 13804-13810, 2014.

[7]. C. Kuznia et al., "Novel high-resolution OTDR technology for multi-Gbps transceivers," *OFC*, W1F.2, pp. 1-3, 2014.

[8]. T. Zhu, X. Xiao, Q. He and D. Diao, "Enhancement of SNR and Spatial Resolution in φ-OTDR System by Using Two-Dimensional Edge Detection Method," *J. Lightwave Technol*. vol. 31, no. 17, pp. 2851-2856, 2013.

[9]. W. Eickhoff and R. Ulrich, "Optical frequency domain reflectometry in single-mode fiber," *Appl. Phys. Lett.*, vol. 39, no. 9, pp. 693–695, 1981.

[10]. Z. Guo, J. Yan, G. Han, D. Greenwood, J. Marco and Y. Yu, "High Sensing Accuracy Realisation With Millimetre/Sub-Millimetre Resolution in Optical Frequency Domain Reflectometer," *J. Lightwave Technol.*, vol. 40, no. 12, pp. 4050-4056, 2022.

[11]. R. Passy, N. Gisin, J. P. von der Weid, and H. H. Gilgen, "Experimental and theoretical investigations of coherent OFDR with semiconductor laser sources," *J. Lightwave Technol.*, vol. 12, no. 9, pp. 1622–1630, 1994.

[12]. Z. Ding, C. Wang, K. Liu, J. Jiang, D. Yang, G. Pan, Z. Pu, and T. Liu, "Distributed Optical Fiber Sensors Based on Optical Frequency Domain Reflectometry: A review" *Sensors*, vol. 18, no. 4, 1072, 2018.

[13]. M. Froggatt and J. Moore, "High-spatial-resolution distributed strain measurement in optical fiber with rayleigh scatter," *Appl. Opt.*, vol. 37, no. 10, pp. 1735–1740, 1998.

[14]. J. Cui, S. Zhao, D. Yang, and Z. Ding, "Investigation of the interpolation method to improve the distributed strain measurement accuracy in optical frequency domain reflectometry systems," *Appl. Opt.*, vol. 57, no. 6, pp. 1424–1431, 2018.

[15]. D. K. Gifford, M. E. Froggatt, A. K. Sang and S. T. Kreger, "Multiple Fiber Loop Strain Rosettes in a Single Fiber Using High Resolution Distributed Sensing," *IEEE Sensors Journal*, vol. 12, no. 1, pp. 55-63,

2012.
[16]. C. Wang, K. Liu, Z. Ding, J. Jiang, Z. Chen, Y. Feng, Y. Zheng, Q. Liu, and T. Liu, “High Sensitivity Distributed Static Strain Sensing Based on Differential Relative Phase in Optical Frequency Domain Reflectometry,” *J. Lightwave Technol.*, vol. 38, no. 20, pp. 5825–5836, 2020.
[17]. W. Feng, M. Wang, H. Jia, K. Xie and G. Tu, "High Precision Phase-OFDR Scheme Based on Fading Noise Suppression," *J. Lightwave Technol.*, vol. 40, no. 3, pp. 900-908, 2022.
[18]. S. Zhao, J. Cui, Z. Wu, Z. Wang and J. Tan, "Distributed Fiber Deformation Measurement by High-Accuracy Phase Detection in OFDR Scheme," *J. Lightwave Technol.*, vol. 39, no. 12, pp. 4101-4108, 2021.
[19]. D. Chen, Q. Liu, and Z. He, "Phase-detection distributed fiber-optic vibration sensor without fading-noise based on time-gated digital OFDR," *Opt. Express*. vol. 25, no. 7, pp. 8315-8325, 2017.
[20]. C. D. Butter and G. B. Hocker, “Fiber optics strain gauge,” *Appl. Opt.*, vol. 17, no. 18, pp. 2867–2869, 1978.
[21]. K. Yuksel, M. Wuilpart, and P. Mégret, “Analysis and suppression of nonlinear frequency modulation in an optical frequency-domain reflectometer,” *Opt. Express*, vol. 17, no. 7, pp. 5845–5851, 2009.
[22]. Z. Guo, G. Han, J. Yan, D. Greenwood, J. Marco, and Y. Yu, “Ultimate spatial resolution realisation in optical frequency domain reflectometry with equal frequency resampling,” *Sensors*, vol. 21, no. 14, 4632, 2021.